Structure of Melittin Bound to Perdeuterated Dodecylphosphocholine Micelles As Studied by Two-Dimensional NMR and Distance Geometry Calculations†

Fuyuhiko Inagaki,*,‡ Ichio Shimada,‡ Ken Kawaguchi,§ Masahiko Hirano,§ Isao Terasawa,§ Teikichi Ikura,∥ and Nobuhiro Gō∥

Department of Molecular Physiology, The Tokyo Metropolitan Institute of Medical Science, 3-18-22 Honkomagome, Bunkyo-ku, Tokyo 113, Japan, Toray Research Center, 1111 Tebiro, Kamakura 248, Japan, and Department of Chemistry, Faculty of Science, Kyoto University, Sakyo-ku, Kyoto, Kyoto 606, Japan

Received December 9, 1988; Revised Manuscript Received March 28, 1989

ABSTRACT: The ^{1}H NMR spectrum of melittin bound to perdeuterated dodecylphosphocholine micelles was analyzed completely by the sequential assignment method with use of two-dimensional NMR techniques. On the basis of the complete sequence-specific resonance assignments, the three-dimensional structure of melittin bound to micelles was determined by distance geometry calculation. Melittin forms an α-helical rod with a kink of 120–160° at Thr11 and Gly12. This rod binds to the micelles with the α-helical axis parallel to the lipid–water interface. The present result is consistent with the "wedge model", where melittin binds to the outer surface of membranes and destabilizes the membrane organization, leading to lysis. However, the above parallel arrangement does not exclude the possibility that melittin is reoriented to a transmembrane position to form a pore when a membrane potential is applied.

Melittin is a major component of the venom of the honey bee, *Apis mellifera* (Habermann, 1972), which comprises 26 amino acid residues: Gly-Ile-Gly-Ala-Val-Leu-Lys-Val-Leu-Thr-Thr-Gly-Leu-Pro-Ala-Leu-Ile-Ser-Trp-Ile-Lys-Arg-Lys-Arg-Gln-Gln-NH_2 (Habermann & Jentsch, 1967). Since melittin has a strong hemolytic activity, its interaction with membranes gives a clue to elucidate its biological activity. Many studies have been made for this purpose using a variety of biophysical methods (Parsegian, 1982; Bernheimer & Rudy, 1986). From the analysis of circular dichroism spectra (Knöppel et al., 1979), melittin takes a random structure in dilute solution, while it takes an α-helical structure in methanol solution or upon binding to lipids. The X-ray structure of melittin tetramer crystallized from aqueous solution was reported (Terwilliger & Eisenberg, 1982; Terwilliger et al., 1982). Melittin monomer is essentially α-helical with a kink around Thr11 and Gly12, which binds together to form a tetramer through hydrophobic interactions, while hydrophilic residues are exposed. However, the molecular structure of melittin bound to lipids and its relative orientation to a lipid–water interface are still unknown, which are important for its hemolytic activity. Here, NMR is the power. Pioneering work by Brown was made to investigate the molecular structure of melittin bound to perdeuterated dodecylphosphocholine (DPC)[1] micelles (Brown & Wüthrich, 1981; Brown et al., 1982). Actually, this study was a milestone for the investigation of the structure of peptides bound to lipids. The use of the perdeuterated micelles eliminates the huge proton resonances from the micelles and also eliminates the spin diffusion effects which obscure the quantitative analysis of NOESY distance information. However, due to a limited number of assignments of the ^{1}H resonances, their conclusion is rather limited. Thus, we started the structural studies of melittin bound to the perdeuterated DPC micelles using 2D NMR and distance geometry calculation. We report here the complete assignment of melittin and the molecular structure of melittin bound to the DPC micelles. Then, we compare the structure of melittin in methanolic solution recently reported by Bazzo et al. (1988) and discuss the physiological activity of melittin on the basis of its molecular structure.

Materials and Methods

Melittin was purchased from Sigma and was further purified with reverse-phase HPLC. Perdeuterated DPC was synthesized according to the method of Brown (1979). Melittin was dissolved at 5 mM concentration in ^2H_2O or H_2O (10% ^2H_2O) with 50 mole ratio of perdeuterated DPC. The pH was adjusted to an uncorrected glass electrode reading (pH*) of 3.5 using a Radiometer PHM86 and and Ingold thin-glass electrode. All the NMR spectra were measured on a JEOL-JNM GX500 ^{1}H 500-MHz NMR spectrometer at 30 °C. 2,2-Dimethyl-2-silapentane-5-sulfonate was used as an internal standard of chemical shifts. DQF-COSY (double-quantum-filtered correlated spectroscopy) (Rance et al., 1983), HOHAHA (homonuclear Hartmann–Hahn spectroscopy) (Bax & Davis, 1985), and NOESY (Jeener et al., 1979; Macura et al., 1981) spectra were recorded in the phase-sensitive mode (States et al., 1982). The water resonance in H_2O spectra was suppressed by selective irradiation during the relaxation delay. For the measurements of NOESY spectra in H_2O, the water resonance was also suppressed by means of the DANTE pulse (Zuiderweg et al., 1986). All two-dimensional spectra were recorded with 512 × 2048 data points and with a spectral width of 6000 Hz. HOHAHA spectra were recorded with a mixing time of 45 ms. NOESY spectra were recorded with mixing times of 80 and 150 ms. Typically, 64–96 scans were accumulated for each t_1 value with relaxation delay of 1.0 s.

† This study was supported through special coordination funds of the Science and Technology Agency, Japan, at Toray Research Center Inc. and at Kyoto University and by a grant-in-aid from the Ministry of Education, Science and Culture of Japan at Kyoto University.

* Author to whom correspondence should be addressed.
‡ The Tokyo Metropolitan Institute of Medical Science.
§ Toray Research Center.
∥ Kyoto University.

[1] Abbreviations: 2D NMR, two-dimensional NMR; DPC, dodecylphosphocholine; DQF-COSY, double-quantum-filtered correlated spectroscopy; HOHAHA, homonuclear Hartmann–Hahn spectroscopy; NOE, nuclear Overhauser effect; NOESY, nuclear Overhauser effect spectroscopy; CD, circular dichroism.

0006-2960/89/0428-5985$01.50/0

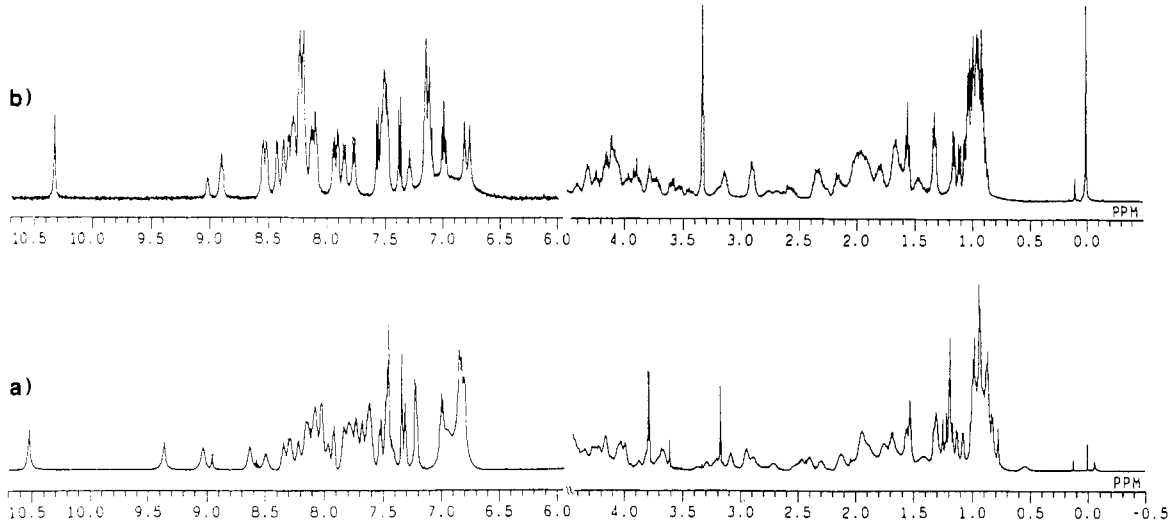

FIGURE 1: 500-MHz ^1H NMR spectrum of melittin (a) bound to the perdeuterated DPC micelles in H_2O solution at pH 3.5 and at 30 °C and (b) in CD_3OH at 30 °C.

The digital resolution was usually 5–6 Hz/point in both dimensions by zero-filling in the t_1 dimension. A phase-shifted sine bell function for DQF-COSY and HOHAHA or a Lorentzian–Gaussian function for NOESY was applied for both t_1 and t_2 dimensions. After Fourier transformations, t_1 ridges were reduced by the subtraction method (Klevit, 1985). Distance geometry calculation was made by using the computer program DADAS (Braun & Gō, 1985) with a FACOM M780 computer at Kyoto University.

Results

Panels a and b of Figure 1 show 500-MHz ^1H NMR spectra of melittin bound to the perdeuterated DPC micelles in H_2O solution and in methanolic solution, respectively. Although melittin was shown to take an α-helical structure in both solutions from CD spectra, there is an appreciable difference between them. It should be noted that the NMR resonances of melittin in the DPC micelles are more dispersed than those in methanolic solution. The difference might be ascribed either to the structural difference of melittin between both environments or to the effect of the lipid–water interface in the micelles which induces significant anisotropic shifts of the proton resonances. Due to the amphiphilic nature of melittin, the lipid–water interface is expected to play important roles for the formation of higher order structure. The relative orientation of melittin to the lipid–water interface as well as its conformation bound to the DPC micelles gives a clue to elucidate its physiological function. Physicochemical properties of the DPC micelles were extensively studied (Brown, 1979; Lauterwein et al., 1979). DPC forms the micelles, comprising 40 molecules, above the critical micelle concentration (1 mM). In the present experimental condition, DPC exists predominantly in the micelle form, and melittin is dispersed in these micelles. We can neglect the aggregation of melittin.

Sequence-specific resonance assignments of melittin in the DPC micelles were made according to the method established by Wüthrich and his co-workers (Wüthrich et al., 1982a). First, the NMR resonances were assigned to the spin systems of specific amino acid types using DQF-COSY and HOHAHA. Second, the spin systems were aligned along the primary structure based on the distance information from the NOESY spectrum.

The fingerprint region of the DQF-COSY spectrum of melittin in the perdeuterated DPC micelles is shown in Figure 2. In spite of the high molecular weight of the complex of melittin and the DPC micelles (23K), the quality of the 2D spectrum was good, and correlation of the chemical shifts of all the amide and α protons in melittin was observed. In addition to these cross-peaks, cross-peaks of $C^{\delta}H_2$, $N^{\epsilon}H$ of arginine residues and $C^{\epsilon}H_2$, $N^{\zeta}H$ of lysine residues, respectively, were also observed (Figure 2) due to the acidic pH condition of the solution, where exchange rates of $N^{\epsilon}H$ and $N^{\zeta}H$ protons with solvent are slow. Melittin contains three lysine and two arginine residues. Although it is generally difficult to assign the side-chain proton resonances of these residues, magnetization transfer starting from $N^{\epsilon}H/N^{\zeta}H$ to other side-chain protons of arginine/lysine residues was observed in the 2D HOHAHA spectrum of melittin bound to perdeuterated micelles in H_2O. Thus, the spin systems of each lysine and arginine residue were assigned (Figure 3). The chemical shift correlations of the amide and α proton resonances were further extended to the side-chain protons using the 2D HOHAHA spectrum of micelle-bound melittin in ^2H_2O. The cross-peaks between the α proton and the side-chain protons were developed as shown in Figure 4, where the spin system of each amino acid type is connected by dashed lines. Each amino acid residue gives a characteristic pattern which in turn gives an assignment of an amino acid type. It is to be noted that magnetization transfer from $C^{\epsilon}H_2$ of lysine and $C^{\delta}H_2$ of arginine residues was also observed, which was then correlated to those from $N^{\zeta}H$ and $N^{\epsilon}H$ protons in H_2O HOHAHA (Figure 3). Thus, all the observable protons were assigned to characteristic spin systems and to specific types of amino acid residues.

Next, the spin systems were aligned according to the primary structure of melittin using distance connectivity by NOESY. Figure 5 shows the NOESY spectrum of the amide proton region of micelle-bound melittin in H_2O. The NOESY cross-peaks due to d_{NN} connectivities were sequentially connected as shown in Figure 5. However, connectivities were interrupted at Pro14 since there is of course no amide proton for the proline residue. In addition, there were interruptions at Ser18-Trp19, and Lys23-Arg24, partly due to the overlap of two amide protons. These interruptions were connected by using $d_{\alpha N}$ and/or $d_{\beta N}$ connectivities. The connectivities thus obtained were also confirmed on the basis of the spin system identifications of the side chains already established through the analysis of the HOHAHA and DQF-COSY spectra. Thus, combined with all 2D NMR data, the complete assignments of melittin bound to the perdeuterated DPC micelles

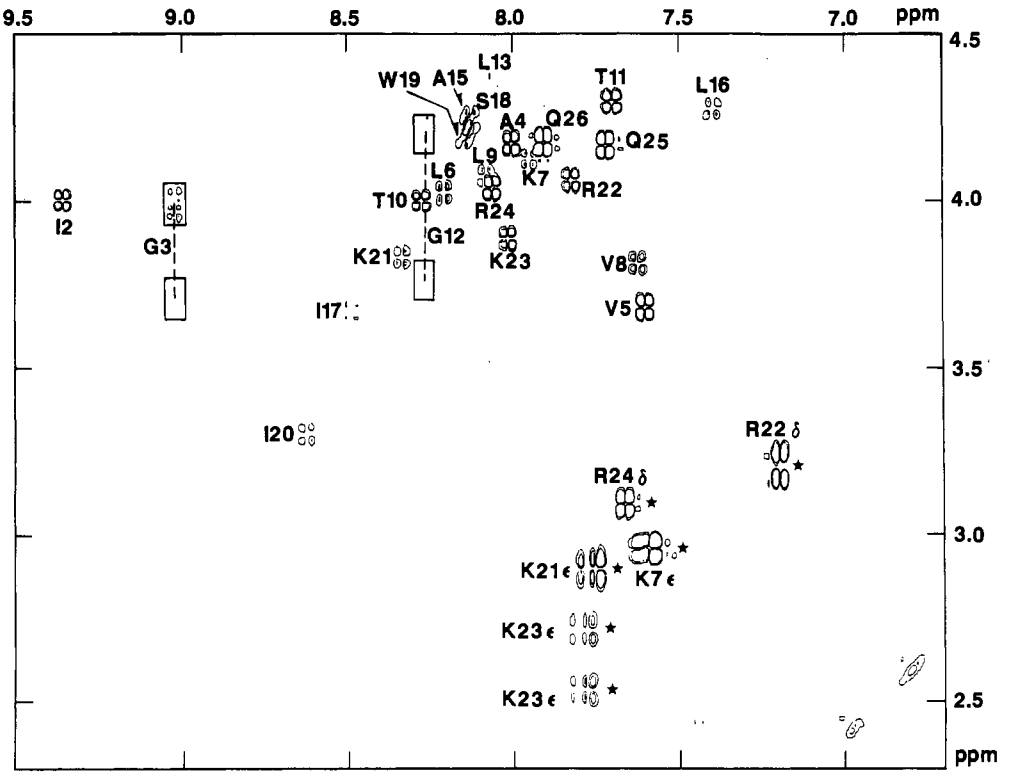

FIGURE 2: Fingerprint region of the DQF-COSY spectrum of melittin in H_2O solution with assigments of the cross-peaks. For a Gly residue, the two cross-peaks $C^{\alpha}H$, NH and $C^{\alpha'}H$, NH are enclosed by boxes and connected by a vertical line. The cross-peaks $C^{\delta}H_2$, $N^{\epsilon}H$ of Arg residues and $C^{\epsilon}H_2$, $N^{\zeta}H$ of Lys residues are shown by stars.

Table I: Chemical Shifts of Proton Resonances of Melittin Bound to DPC Micelles at 30 °C and pH 3.5[a]

	chemical shift (ppm)			
residue	NH	$C^{\alpha}H$	$C^{\beta}H$	others
Gly1		4.04, 3.92		
Ile2	9.35	4.00	1.93	$C^{\gamma}H$ 1.59, 1.31; $C^{\gamma}_{M}H$ 1.00; $C^{\delta}H$ 0.95
Gly3	9.01	3.99, 3.71		
Ala4	8.00	4.17	1.53	
Val5	7.60	3.67	2.30	$C^{\gamma}H$ 1.07, 0.94
Leu6	8.21	4.01	1.87, 1.64	$C^{\gamma}H$ 1.87; $C^{\delta}H$ 0.95, 0.88
Lys7	7.95	4.12	1.96, 1.96	$C^{\gamma}H$ 1.54, 1.47; $C^{\delta}H$ 1.70, 1.70; $C^{\epsilon}H$ 2.96, 2.96; $N^{\zeta}H$ 7.60
Val8	7.62	3.80	2.31	$C^{\gamma}H$ 1.14, 0.98
Leu9	8.09	4.07	1.96, 1.96	$C^{\gamma}H$ 1.92; $C^{\delta}H$ 0.87, 0.83
Thr10	8.28	3.99	4.33	$C^{\gamma}H$ 1.33
Thr11	7.20	4.28	4.28	$C^{\gamma}H$ 1.31
Gly12	8.27	4.22, 3.74		
Leu13	8.05	4.35	1.97, 1.76	$C^{\gamma}H$ 1.84; $C^{\delta}H$ 0.99, 0.94
Pro14		4.27	2.40, 1.95	$C^{\gamma}H$ 2.28, 2.03; $C^{\delta}H$ 3.72, 3.63
Ala15	8.13	4.28	1.55	
Leu16	7.40	4.26	2.15, 1.63	$C^{\gamma}H$ 1.74; $C^{\delta}H$ 1.01, 0.91
Ile17	8.48	3.67	2.03	$C^{\gamma}H$ 1.75, 1.23; $C^{\gamma}_{M}H$ 0.97; $C^{\delta}H$ 0.89
Ser18	8.15	4.22	4.09, 4.05	
Trp19	8.14	4.23	3.70, 3.37	N1H 10.53; C2H 7.33; C4H 7.52; C6H 6.98; C7H 7.46
Ile20	8.62	3.29	2.11	$C^{\gamma}H$ 2.25, 1.23; $C^{\gamma}_{M}H$ 0.90; $C^{\delta}H$ 0.93
Lys21	8.33	3.82	1.90, 1.90	$C^{\gamma}H$ 1.69, 1.40; $C^{\delta}H$ 1.69, 1.69; $C^{\epsilon}H$ 2.90, 2.90; $N^{\zeta}H$ 7.75
Arg22	7.82	4.06	1.90, 1.54	$C^{\gamma}H$ 1.80, 1.73; $C^{\delta}H$ 3.20, 3.20; $N^{\epsilon}H$ 7.19
Lys23	8.01	3.87	1.40, 1.40	$C^{\gamma}H$ 0.85, 0.55; $C^{\delta}H$ 1.31, 1.31; $C^{\epsilon}H$ 2.71, 2.54; $N^{\zeta}H$ 7.78
Arg24	8.06	4.02	1.97, 1.78	$C^{\gamma}H$ 1.64, 1.64; $C^{\delta}H$ 3.09, 3.09; $N^{\epsilon}H$ 7.65
Gln25	7.72	4.15	2.14, 1.97	$C^{\gamma}H$ 2.48, 2.42; $N^{\epsilon}H$ 7.46, 6.78
Gln26	7.91	4.16	2.13, 2.04	$C^{\gamma}H$ 2.46, 2.38; $N^{\epsilon}H$ 7.43, 6.83
$CONH_2$	7.31, 7.22			

[a] Chemical shifts are measured to ±0.01 ppm.

were accomplished, and are shown in Table I. The high-field-shifted broad resonance at 0.55 ppm is now assigned to one of the γ-methylene protons of Lys23. Unusual high-field shift of this proton should be elucidated on the basis of the three-dimensional structure of melittin bound to the DPC micelles.

The NOESY cross-peaks were subsequently analyzed on the basis of complete assignments of the proton resonances of melittin bound to DPC micelles. Figure 6 shows the NOESY spectrum of micelle-bound melittin in the cross-peak region of the α and aliphatic proton resonances. In addition to the NOESY cross-peaks due to intraresidue protons, the $d_{\alpha\beta}(i, i+3)$ connectivities were observed as are enclosed in Figure 6. Figure 7 summarizes the distance connectivities for melittin bound to the perdeuterated DPC micelles. It should be noted here that the NOE connectivities with more than five

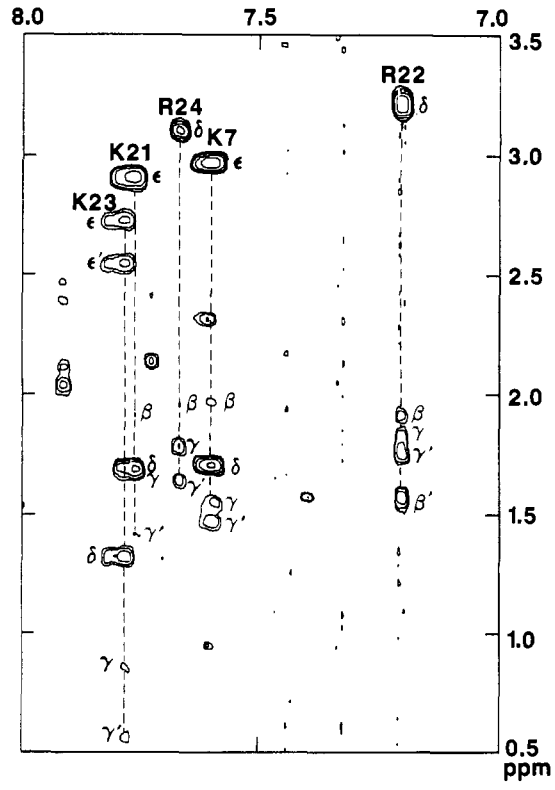

FIGURE 3: HOHAHA spectrum of melittin in the cross-peak region of aliphatic proton, $N^{\epsilon}H$ of Arg residues and aliphatic proton, $N^{\zeta}H$ of Lys residues in H_2O solution with a mixing time of 45 ms. The spin system of each of the Arg and Lys residues is connected by a dashed line with the assignment of each proton resonance.

residues apart were not observed, showing that melittin bound to the DPC micelles does not take a folded conformation but rather takes an extended rod. The distance connectivities suggested that melittin bound to the DPC micelles takes an α-helical structure (Wüthrich, 1986). However, the α-helical structure was expected to be distorted due to the presence of Pro14. From the $d_{\alpha\delta}$ connectivity, the peptide bond between Leu13 and Pro14 was found to take a trans form.

Next, the distance geometry calculation was made on the basis of the distance constraints obtained from the analysis of the NOESY spectra. A total of 68 intraresidue NOEs, 93 NOEs between neighboring residues and 70 of other NOEs, were used as distance constraints. The constraints were obtained by classifying NOESY cross-peak intensities into four categories based on counting the contour levels in the NOESY spectrum. The NOEs and distance constraints were classified into four groups: strong (<0.25 nm), medium–strong (<0.30 nm), medium (<0.35 nm), and weak (<0.40 nm), according to the intensity of the NOESY cross-peaks of known proton–proton distances. Distance corrections were then made by means of the pseudoatom presentation (Wüthrich et al., 1982b). Since there were no NOE connectivities between amino acid residues with more than five residues apart, melittin was divided into five fragments: Gly1–Leu6, Val5–Gly12, Thr10–Ile17, Pro14–Lys21, and Trp19–Gln26. Starting from 20 initial structures generated from randomly selected dihedral angles, the global minimum of the variable target function was searched for each fragment by using the computer program DADAS. Then, each fragment was combined together successively from the N-terminal segment, which was subsequently applied to the distance geometry calculations to finally find the global structure of the melittin molecule. Figure 8 shows a representative structure of melittin bound to the micelles. The root mean square (rms) deviation of the individual segments of Gly1–Thr10 and Leu13–Gln26 for the backbone atoms of the obtained structures was 0.17 and 0.13 nm, respectively, showing that the structure of each segment was well-defined. Although both segments take helical structures, the bent angle between the two segments was not uniquely determined and varied from 120° to 160°. However,

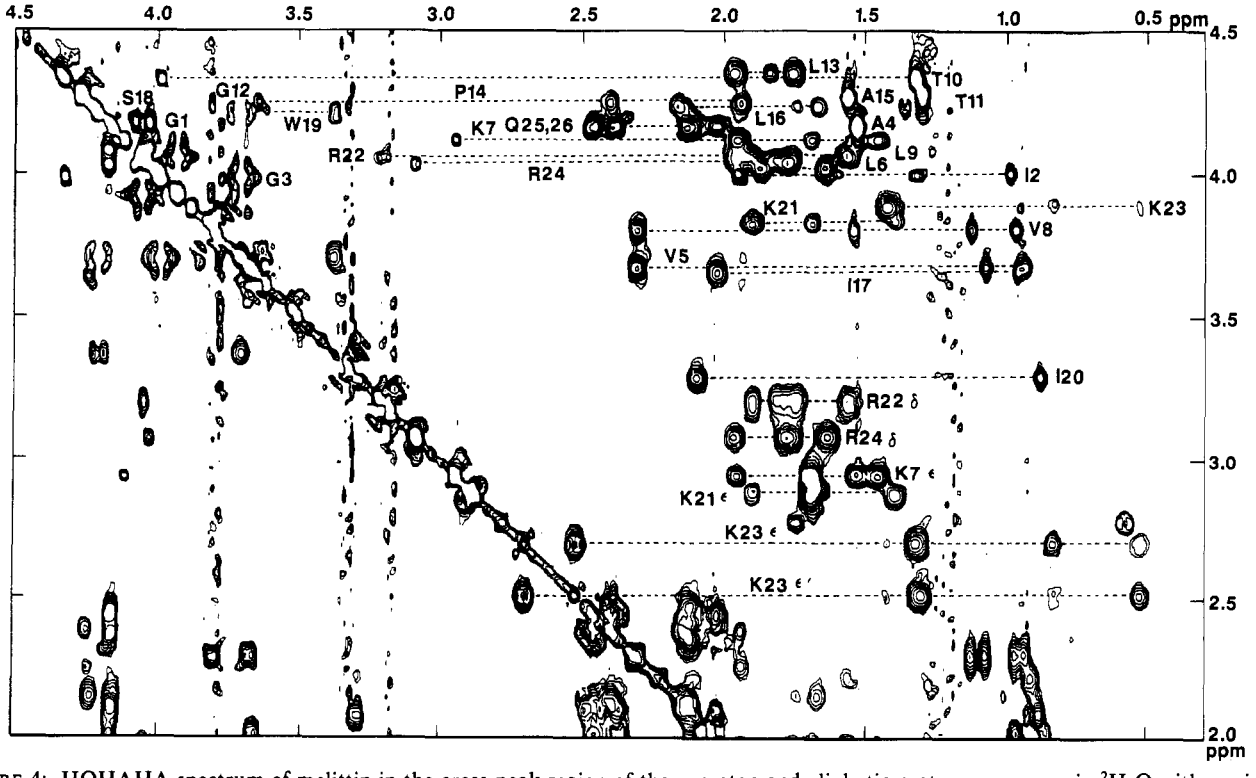

FIGURE 4: HOHAHA spectrum of melittin in the cross-peak region of the α proton and aliphatic proton resonances in ^2H_2O with a mixing time of 45 ms. The spin system of each amino acid residue is connected by a dashed line at the chemical shifts of the α-proton resonance. Spin systems developed from $C^{\delta}H_2$ of Arg residues and $C^{\epsilon}H_2$ of Lys residues are also shown as dashed lines.

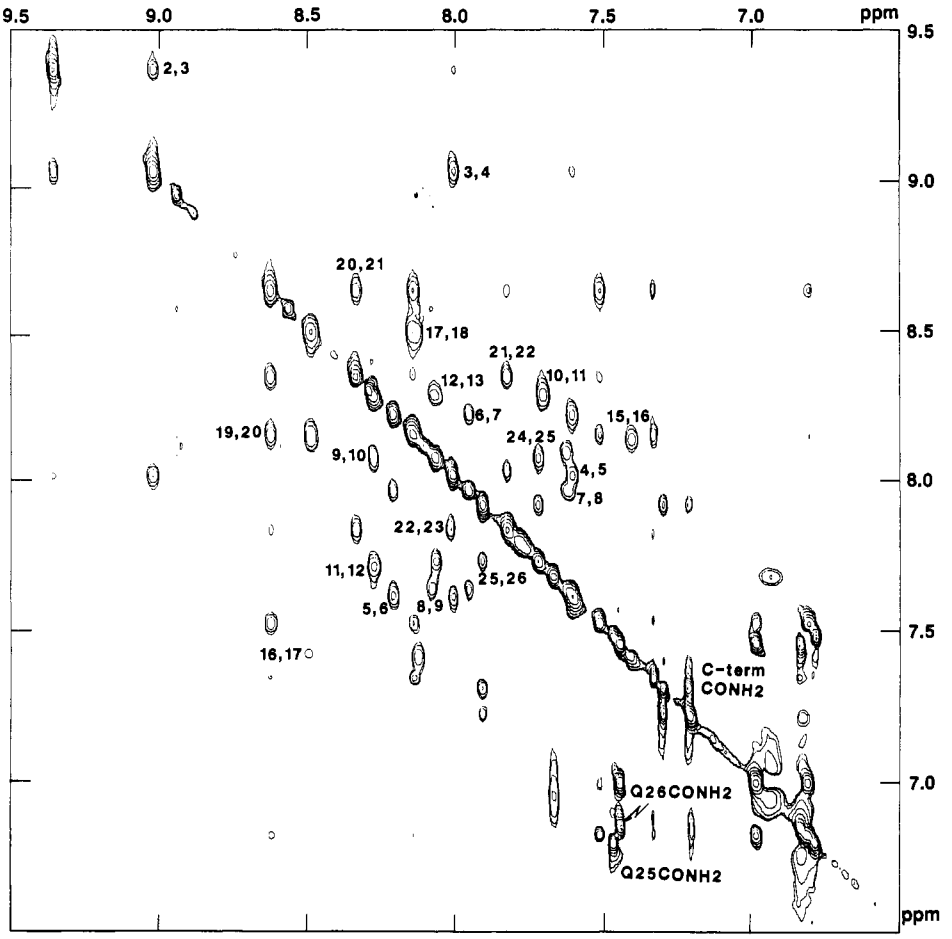

FIGURE 5: Amide proton region of the NOESY spectrum of melittin with a mixing time of 150 ms. NOESY cross-peaks due to the d_{NN} connectivities are labeled with the residue numbers of the corresponding amino acids. Carboxamide protons of C-terminal and glutamine side chains are also shown.

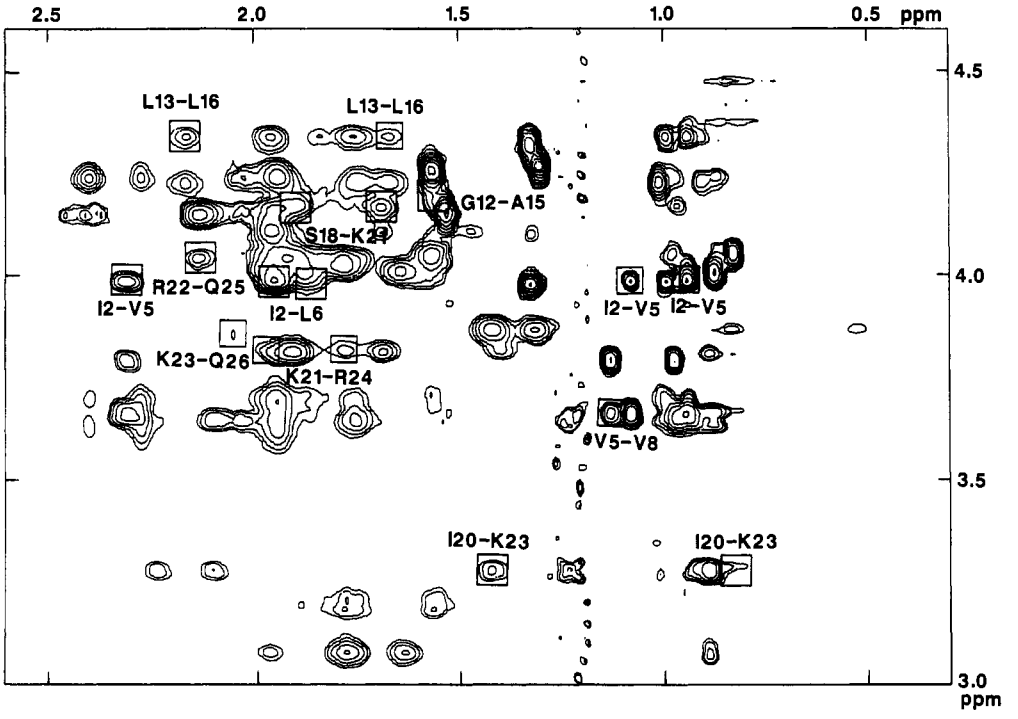

FIGURE 6: Cross-peak region of the α and aliphatic proton resonances of the NOESY spectrum with a mixing time of 150 ms. The NOESY cross-peaks due to the distance connectivities of $d_{\alpha\beta}$ $(i, i + 3)$ are enclosed by boxes.

the present results show that the above procedure starting from the fragments to combine the whole structure is quite efficient to decrease the amount of computation time and is also useful to avoid the local minimum problem at least in the case of melittin. It should be noted that the side chain of Lys23 is close to the indole ring of Trp19, which is consistent with the

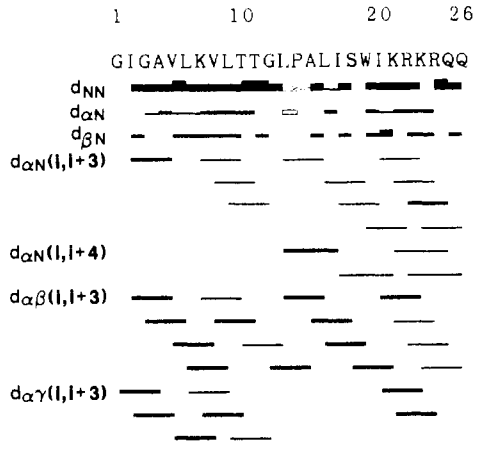

FIGURE 7: Distance connectivities observed for melittin bound to the DPC micelles. Instead of d_{NN}, $d_{N\delta}$ and $d_{\delta N}$ were used for the connectivity of Leu13-Pro14 and Pro14-Ala15, respectively. For Leu13-Pro14, $d_{\alpha\delta}$ was observed, showing that the peptide bond between Leu13 and Pro14 takes a trans form.

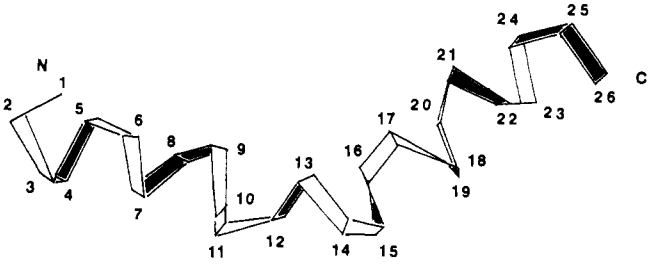

FIGURE 8: Representative structure of melittin bound to the micelles derived from distance geometry calculations. The N-terminal and C-terminal segments take α-helical structures with a kink at Thr11 and Gly12. The bent angle is 120°.

high-field shift of $C^{\gamma}H_2$ of Lys23 (Table I).

Discussion

The structure of melittin in the DPC micelles was initially determined by Brown et al. using 2D NMR and distance geometry calculations (Brown et al., 1982). Although this work was a pioneering work for the conformation study of peptides bound to the micelles, the results are rather limited partly due to the lack of assignments. After they took several possibilities for the assignments of Ile and Lys residues into account, they concluded that the N-terminal and the C-terminal segments of melittin form two spatially distinct, compact domains, where the C-terminal domain takes the α-helical structure. However, they did not know anything on the N-terminal domain. They also proposed, using lipid spin-labels, that melittin is located near the micelle surface rather than penetrating into the interior of the micelles.

In the present study, we have determined the conformation of melittin bound to DPC micelles. Melittin assumes a rodlike α-helical conformation which has a kink at Thr11 and Gly12 with a bent angle of 120–160°, as shown in Figure 8. The structure of melittin bound to the DPC micelles was found to be more regular than those previously reported (Brown et al., 1982) and was in good agreement with the structure of melittin in the crystalline state, which has a bent angle of 120°. However, the top part of the C-terminal segment still takes a helical structure but is slightly distorted due to irregularity of the helix around the kink (Figure 8). This is shown in Figures 5 and 7, where irregular connectivity of d_{NN} at Leu16-Ile17 was observed (the disruption of d_{NN} connectivity at Ser18-Trp19 is due to overlap of the amide proton resonances). There is another structural disorder at Lys23-Arg24

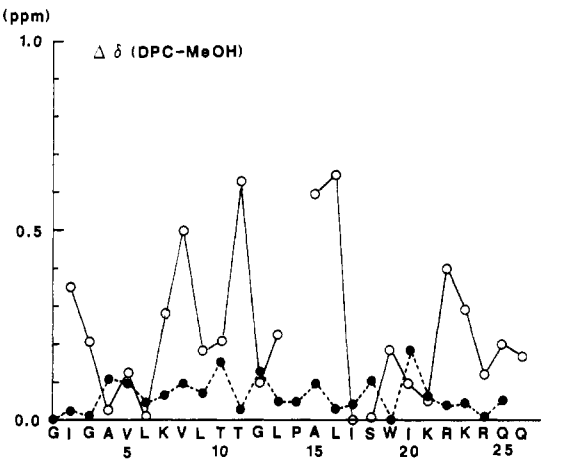

FIGURE 9: Difference of the chemical shifts of the amide (solid line) and α (dashed line) proton resonances between two environments of DPC micelles and methanolic solution in absolute values.

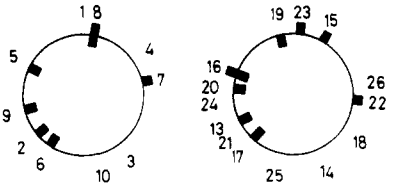

FIGURE 10: Helical wheels of the two α-helical segments 1–10 and 13–26 in the structure shown in Figure 8. Clusterings of residues showing strong hydrophobicity (marked inside the wheels) and significant chemical shift changes (marked outside the wheels) are clearly seen in the wheels.

manifested in the absence of the d_{NN} cross-peak (Figure 5), which may be essential for keeping the C-terminal positively charged groups into hydrophilic environments. Recently, the conformation of melittin in methanolic solution was determined by NMR (Bazzo et al., 1988). It should be noted that the structure of melittin in methanolic solution also takes the α-helical structure with the bent angle of 160°. In the present study, the bent angle was not uniquely determined due to lack of a sufficient number of NOESY data. Since a hydrogen bond is not formed between Thr10 and Pro14, melittin is expected to be flexible around Thr11 and Gly12. It was expected that large curvature of the micelle distorts the intrinsic structure of melittin. However, since the molecular structures of melittin in the crystalline state, in methanolic solution, and in the micelles are similar, the micelles are expected to conform to the structure of melittin rather than melittin conforming to the curvature of the micelles. When we compared the chemical shifts of the proton resonances of melittin, one in methanolic solution and the other bound to the micelles (Bazzo et al., 1988), some amide proton resonances shifted significantly to higher or lower field. The difference may be due to the presence of the lipid–water interface in the micelles, compared to the isotropic environment of the methanolic solution. Figure 9 shows the difference of the chemical shifts of the amide and α-proton resonances between two environments in absolute values. A significant difference was observed for the amide proton resonances of Lys7, Val8, Thr11, Ala15, Leu16, Arg22, and Lys23. While the chemical shifts of α-proton resonances did not change significantly for both states, amide protons were more sensitive to the change of the environments from the micelles to methanolic solution. Actually, when the amide protons which show significant chemical shift changes are plotted on the three-dimensional structure of melittin shown in Figure 8, these amide protons are located on the one surface of the melittin

molecule (Figure 10). Except for the Leu16 residue, mainly hydrophilic residues are located on this side, while hydrophobic residues such as Ile2, Val5, Leu6, Leu9, Leu13, Ile17, and Ile20 are located on the other side. From comparison of the data obtained in the two environments, it was concluded that melittin binds to the lipid–water interface where the hydrophilic residues are exposed to water, while the hydrophobic residues penetrate into the interior of the micelles. The orientation of melittin relative to the lipid–water interface was also supported by the amide proton exchange studies, where the melittin–DPC complex (1:50) lyophilized from H_2O solution was dissolved in ^2H_2O solution. Upon dissolution of the lyophilized sample in ^2H_2O solution at 30 °C, the amide proton resonances of Ile2, Gly3, Ala4, Lys7, Thr10, Thr11, Gly12, Leu16, Gln25, and Gln26 exchanged rapidly with solvent, while those of Val5, Leu6, Leu9, Leu13, Ile17, Trp19, Ile20, Lys21, and Arg22 were slowly exchanged with solvent. Especially, the exchange rates of the amide protons of Leu9, Leu13, Ile17, Ile20, and Lys21 were extremely slow so that these amide protons were observed for 2 days after the sample preparation in ^2H_2O solution. The slowly exchangeable amide protons were found to be mainly located on the hydrophobic surface and the fast-exchangeable amide protons to be located on the hydrophilic surface of the melittin molecule. If this experimental evidence is combined together, melittin binds to the lipid–water interference of the DPC micelles with the helix axis parallel to the micelle surface, as was initially suggested by Brown et al. (1982).

There have been controversies in the literature about the orientation of the α-helical segments of melittin relative to the lipid bilayer membrane surface. Some postulate that the α-helical axis is perpendicular to the membrane surface, where melittin penetrates deeply into the bilayer and Lys7 is buried in the membrane (Vogel et al., 1983, 1986). Others conclude that melittin binds to the membranes with its axis parallel to the membrane surface, and Lys7 is exposed to the aqueous phase (Brown et al., 1982; Dawson et al., 1978; Terwilliger et al., 1982). A more differentiated model shows a binding parallel to the surface, which in turn changes to a perpendicular orientation when a transmembrane voltage is applied (Kempf et al., 1982; Hanke et al., 1983). Quenching of fluorescence of Trp19 by acrylamide shows that Trp19 is located near the surface rather than deeply embedded in the micelles (Georghiou et al., 1982). Moreover, recent ESR studies show that Lys7 is most exposed to the solvent, following Lys23 and Lys21 (Altenbach & Hubbell, 1988). These studies support that melittin binds to the surface of the membrane. The ESR study also shows that melittin binds to the membrane in a monomeric form rather than an aggregated form (Altenbach & Hubbell, 1988). Thus, the structure of melittin in the micelles and its relative orientation to the lipid–water interface give a good model for those bound to the membrane. The present result supports the "wedge" model for lytic activity of melittin; melittin binds to the outer surface of the membrane which results in increase of the membrane curvature and gives a driving force for formation of lipid pores or for rupturing the membrane (Dawson et al., 1978; Brown et al., 1982; Terwilliger et al., 1982). Of course, the present result does not rule out the possibility of a voltage-dependent transmembrane orientation of melittin, where the induced large α-helical dipole changes the orientation of melittin from parallel to a transmembrane position through the membrane potential, forming a pore as a tetramer (Kempf et al., 1982; Hanke et al., 1983). However, for both models, the initial step is the formation of α-helical structure upon the membrane surface as elucidated in the present study from the random structure in aqueous solution. The use of perdeuterated micelles for conformation study of membrane-bound peptides combined with 2D NMR techniques is useful for elucidation of their biological activities and is also useful for drug design.

Registry No. DPC, 29557-51-5; melittin, 20449-79-0.

References

Altenbach, C., & Hubbell, W. L. (1988) *Proteins: Struct., Funct., Genet. 3*, 230–242.

Bax, A., & Davis, D. G. (1985) *J. Magn. Reson. 65*, 393–402.

Bazzo, R., Tappin, M. J., Postore, A., Harvey, T. S., Carver, J. A., & Campbell, I. D. (1988) *Eur. J. Biochem. 173*, 139–146.

Bernheimer, A. W., & Rudy, B. (1986) *Biochim. Biophys. Acta 864*, 123–141.

Braun, W., & Gō, N. (1985) *J. Mol. Biol. 186*, 611–626.

Brown, L. R. (1979) *Biochim. Biophys. Acta 557*, 135–148.

Brown, L. R., & Wüthrich, K. (1981) *Biochim. Biophys. Acta 647*, 95–111.

Brown, L. R., Braun, W., Kumar, A., & Wüthrich, K. (1982) *Biophys. J. 37*, 319–328.

Dawson, C. R., Drake, A. F., Helliwell, J., & Hilder, R. C. (1978) *Biochim. Biophys. Acta 510*, 75–86.

Georghiou, S., Thompson, S. G. M., & Mukhopadhyay, A. K. (1982) *Biochim. Biophys. Acta 688*, 441–452.

Habermann, E. (1972) *Science 177*, 314–322.

Habermann, E., & Jentsch, J. (1967) *Hoppe Seyler's Z. Physiol. Chem. 348*, 37–50.

Hanke, W., Methfessel, C., Wilmsen, H. U., Katz, E., Jung, G., & Boheim, G. (1983) *Biochim. Biophys. Acta 727*, 108–114.

Jeener, J., Meier, B. H., Bachmann, P., & Ernst, R. R. (1979) *J. Chem. Phys. 71*, 4546–4553.

Kempf, C., Klausner, R. D., Weinstein, J. N., Renswoude, J. V., Pincus, M., & Blumenthal, R. (1982) *J. Biol. Chem. 257*, 2469–2476.

Klevit, R. E. (1985) *J. Magn. Reson. 62*, 551–555.

Knöppel, E., Eisenberg, D., & Wickner, W. (1979) *Biochemistry 18*, 4177–4181.

Lauterwein, J., Bösch, C., Brown, L. R., & Wüthrich, K. (1979) *Biochim. Biophys. Acta 556*, 244–264.

Macura, S., Huang, Y., Suter, D., & Ernst, R. R. (1981) *J. Magn. Reson. 43*, 259–281.

Parsegian, V. P. (1982) *Biophys. J. 37*, 3–411.

Rance, M., Sørensen, O. W., Bodenhausen, G., Wagner, G., Ernst, R. R., & Wüthrich, K. (1983) *Biochem. Biophys. Res. Commun. 117*, 479–485.

States, D. J., Haberkorn, R. A., & Ruben, D. J. (1982) *J. Magn. Reson. 48*, 286–292.

Terwilliger, T. C., & Eisenberg, D. (1982) *J. Biol. Chem. 257*, 6016–6022.

Terwilliger, T. C., Weissman, L., & Eisenberg, D. (1982) *Biophys. J. 37*, 353–361.

Vogel, H., & Jähnig, F. (1986) *Biophys. J. 50*, 573–582.

Vogel, H., Jähnig, F., Hoffmann, V., & Stümpel, J. (1983) *Biochim. Biophys. Acta 733*, 201–209.

Wüthrich, K. (1986) in *NMR of Proteins and Nucleic Acids*, Wiley, New York.

Wüthrich, K., Wider, G., Wagner, G., & Braun, W. (1982a) *J. Mol. Biol. 155*, 311–319.

Wüthrich, K., Billeter, M., & Braun, W. (1982b) *J. Mol. Biol. 169*, 949–961.

Zuiderweg, E. R. P., Hallenga, K., & Olejniczak, E. T. (1986) *J. Magn. Reson. 70*, 336–343.